ACS Photonics

Article

pubs.acs.org/journal/apchd5

On the Nonlocal Response of Multilayer Optical Metamaterials

Rasta Ghasemi, Xavier Le Roux, Anatole Lupu, André de Lustrac, and Aloyse Degiron*

Institut d'Electronique Fondamentale, UMR 8622, CNRS, University of Paris Sud, 91405 Orsay, France

ABSTRACT: We provide a microscopic description of a three-dimensional infrared metamaterial composed of stacked arrays of gold cut wires buried in a dielectric host. We show with numerical and theoretical arguments that the response of this structure is intrinsically nonlocal and explain why this property makes it robust to fabrication errors such as misalignments between adjacent levels of cut wires. We then validate these claims by fabricating and characterizing experimental samples comprising up to four layers of cut wires. These results relax the fabrication tolerances of bulk optical metamaterials composed of strongly interacting layers and also imply that their effective parameters cannot be inferred from retrieval methods based on a purely local description of the permittivity and permeability.

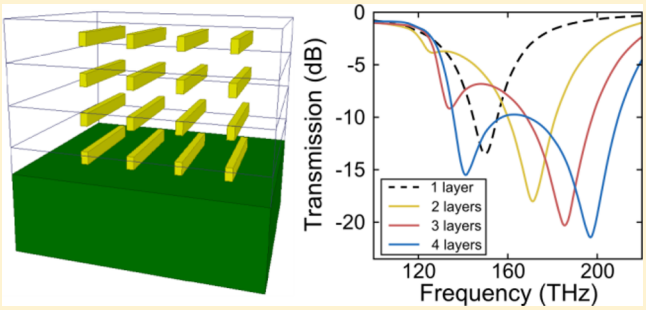

KEYWORDS: *optical metamaterials, surface plasmon resonances, three-dimensional nanocomposites*

The development of three-dimensional optical metamaterials (MMs) has been challenging due to the many physical and technological roadblocks that are encountered in their fabrication.[1] One of the most widely investigated architectures, the negative-index fishnet MM, is also probably the most compatible with current nanofabrication tools because its making requires only a single step of electron-beam or laser lithography.[2,3] Recent articles have shown that fishnet MMs can also be fabricated with laser interference lithography[4] or nanotransfer printing,[5] enabling large-scale production with minimal efforts. Other useful approaches for fabricating 3D optical MMs include direct laser printing[6] (which is especially suited for fabricating chiral structures, although the minimum feature size is limited by the wavelength used for writing) as well as self-assembled techniques, for example by using block copolymers and metal electrodeposition.[7] It is even possible to fabricate useful three-dimensional MMs without any nanostructuration step, as is the case for instance with hyperbolic uniaxial media that are obtained by coating alternating layers of dielectrics and metals.[8]

None of these approaches, however, are well adapted to the fabrication of MMs whose permittivity and permeability can be independently controlled and varied across the volume of the composite, a much needed characteristic for transformation optical components, for example, i.e., artificial media that behave as if space itself were distorted.[9] To date, two main classes of optical MMs are potentially compatible with transformation optics. For devices operating with gradients in their refractive index only, it is possible to utilize 2D or 3D photonic crystals in the homogenization regime, as was done for example with various "carpet" cloaks capable of minimizing the scattering of an object above a ground plane.[10−12] For applications requiring an independent control of both the permittivity and permeability, one can rely on structures derived from radio frequency MMs that typically consist of 3D assemblies of highly subwavelength metallic inclusions. Fabricating such MMs is usually achieved by adopting a layer-by-layer strategy whereby stacks of nanoparticle arrays are fabricated by successive steps of electron-beam lithography, metal deposition, lift-off, and application of a dielectric spacer.[13−19]

Contrarily to many of their low-frequency counterparts, the response of multilayer MMs operating in the optical regime arises not only from their individual unit cells but also from the coupling between each plane of inclusions.[13,14,17−19] While such interactions offer an extra degree of freedom for designing the structures, they also come with difficulties of their own. For example, it is generally accepted that a careful alignment of all layers is a requisite for high-quality samples, considerably complicating the fabrication process.[15,18,19] It would be therefore desirable to identify structures that are not affected by this problem. Moreover, the role played by interacting layers in the MM effective response is only partially understood, especially in the case of structures made of strongly coupled elements.

In this paper, we address these questions for an archetypical multilayer geometry: a periodic stack of gold cut wire (CW) arrays separated by dielectric spacers. We provide a microscopic description of the propagation through this artificial medium with numerical simulations, temporal coupled mode theory, and experiments on samples made of up to four layers of CWs. We show that their spectral signature and effective material parameters can be explained only if the interactions between planes of CWs go beyond first-neighbor coupling. We also demonstrate at the same time that their optical properties are

Received: April 7, 2015
Published: July 2, 2015

DOI: 10.1021/acsphotonics.5b00180
ACS Photonics 2015, 2, 1129−1134

very robust to disorder, relaxing the fabrication tolerances of future samples.

The MM geometry is schematically represented in Figure 1a. Each layer consists of a periodic array of gold cut wires

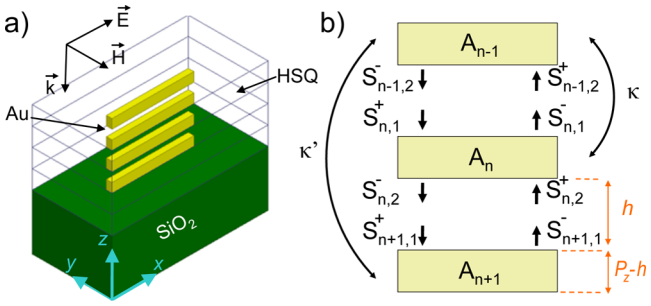

Figure 1. (a) General view of the multilayer metamaterial. This unit cell is periodically reproduced along the x and y directions, and the structure is illuminated by a plane wave polarized with the electric field along the length of the CWs. (b) Schematic view of the quantities used in eq 1 (the coupling constants κ'', $\kappa^{(3)}$, ..., $\kappa^{(i-1)}$ between third, fourth, ..., and ith neighbors are not represented).

embedded in hydrogen silsesquioxane (HSQ), a sol–gel glass offering good surface planarization and high process reproducibility and characterized by a permittivity (ε_{HSQ} = 1.96) close to that of the silica substrate onto which the structures are fabricated (ε_{SiO2} = 2.2).

To understand the behavior of multilayer structures, it is quite instructive to briefly review the properties of MMs composed of two planes of CWs only. For this purpose, we modeled a series of bilayer structures with increasing separation distances h between the planes of CWs in HFSS, a commercial software based on the finite element method.[20] The length of the CWs is L = 440 nm, the width W = 30 nm, and the thickness T = 50 nm. The period in the x direction along the wires is P_x = 840 nm and in the y direction perpendicular to the wires P_y = 430 nm. For the dielectric permittivity of gold, we use a Drude model with the same parameters as in ref 21. All the calculations discussed in this article were performed under normal plane wave incidence polarized along the x axis (electric field E parallel to the CWs). Importantly, we have verified that these results remain true for a range of incident angles corresponding to the illumination cone of the experiments presented in the last part of the study. To provide a homogeneous dielectric environment, the top level of CWs is covered with a 100 nm thick HSQ overclad.

Figure 2a compares the transmission spectra of the bilayer structures with the response of a single array of CWs of the same dimensions and periodicity. Given the geometrical parameters considered in our study, the isolated array presents a single resonance centered at 150 THz that corresponds to the fundamental localized plasmon resonance of the CWs.[17] In contrast, the bilayer structures exhibit two dips in their spectral response resulting from the hybridization between the two planes of CWs. The low-frequency mode has been the object of considerable interest in the literature because it is characterized by an antisymmetric distribution of the vertical component of the electric field and by out-of-phase current oscillations. This electromagnetic configuration makes it possible to excite the resonance by the magnetic field only, imparting an effective magnetic permeability different from unity to the whole structure.[13,14] In contrast, the high-frequency mode is

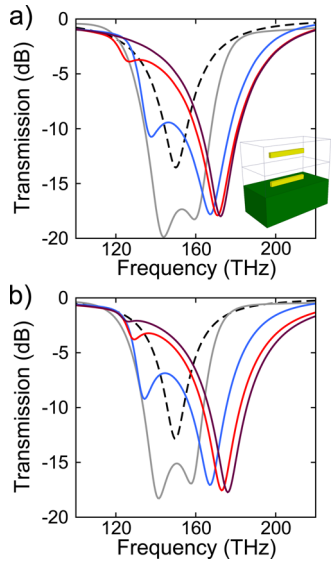

Figure 2. (a) Full-wave transmission spectra of a series of bilayer structures. The CW dimensions are 440 × 30 × 50 nm, while the separation distance between the CWs is successively set to h = 350 nm (gray curve), h = 150 nm (blue curve), h = 50 nm (red curve), and h = 10 nm (indigo curve). The periods along the x and y axes are P_x = 840 nm and P_y = 430 nm, respectively. The spectrum of a single array of CWs is added for comparison (black dashed curve). (b) Response of the same structures according to temporal coupled mode theory.

essentially an electric dipole acting on the effective permittivity of the sample. Figure 2a shows that the splitting of the resonances increases from 15 THz to 80 THz as the separation h decreases from 350 nm to 10 nm; in addition, the amplitude of the low-energy peak gradually vanishes, while the strength of the high-energy peak remains fairly constant. This trend can be explained by the fact that, as h tends to zero, each pair of coupled resonators merges into a unique CW with a new resonance at a higher frequency.

We now examine how this well-know response evolves as new arrays of CWs are stacked on the structure. Because adding more layers amounts to increasing the number of coupled resonances in the system, one would expect to see the spectral signature of these new eigenmodes. However, as evidenced by Figure 3a, the transmission spectra of MMs with two, three, and four layers of CWs look very much alike in this example, where the layers are separated by a distance h = 50 nm. All structures feature only two minima in their transmission spectra, and the only noticeable difference between the various curves is that the peaks shift to higher energies and their amplitudes become more pronounced as the number of layers increases.

To explain this result, we have duplicated the spectra of Figures 2a and 3a with analytical equations based on the temporal coupled mode theory.[22] Generalizing the work of ref 23 for a bilayer of photonic crystals, we write the response of the multilayer structure as

DOI: 10.1021/acsphotonics.5b00180
ACS Photonics 2015, 2, 1129–1134

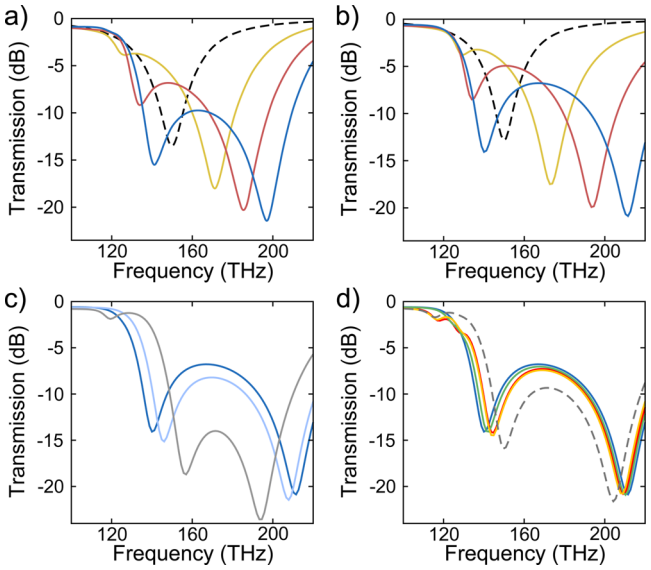

Figure 3. (a) Full-wave transmission spectra for structures composed of one, two, three, and four layers of CWs (black-dashed curve, yellow, red, and blue, respectively). The separation distance between each plane of CWs is set to h = 50 nm (corresponding to a period P_z = 100 nm); the other parameters are the same as those considered in Figure 2. (b) Response of the same structures according to temporal coupled mode theory. (c) Transmission of the ideal four-layer structure of part b (blue curve) compared with the calculations with third-neighbor coupling disabled (κ'' = 0, light blue curve) and with both third- and second-neighbor interactions disabled (κ'' = κ' = 0, gray curve). (d) Transmission of the ideal four-layer structure of part b (blue curve) compared with calculations made with several types of disorder. Red curve: Each layer has a different resonance frequency (ν_1 = 159 THz, ν_2 = 135 THz, ν_3 = 150 Thz, and ν_4 = 148.5 Thz). Green curve: Adjacent layers have different first-neighbor coupling constants (1.2 κ, 0.8 κ, and 0.9 κ). Yellow curve: Calculation combining the two types of disorder. Gray dashed curve: Same as yellow, but with third-neighbor interactions disabled.

$$\begin{cases} [j(\omega-\omega_0)+\Gamma_{tot}]A_n \\ \quad = \alpha S^+_{n,1} + \alpha S^+_{n,2} + j\kappa A_{n\pm1} + j\kappa' A_{n\pm2} + \ldots \\ \quad\quad + j\kappa^{(i-1)} A_{n\pm i} \\ S^-_{n,2} = tS^+_{n,1} + rS^+_{n,2} + \alpha A_n \\ S^-_{n,1} = tS^+_{n,2} + rS^+_{n,1} + \alpha A_n \\ S^+_{n,1} = S^-_{n-1,2}\exp(-jn_{HSQ}h\omega/c) \\ S^-_{n,1} = S^+_{n-1,2}\exp(+jn_{HSQ}h\omega/c) \end{cases} \quad (1)$$

where ω_0 and Γ_{tot} are the angular resonance frequency and the total decay rate of the isolated resonator, t and r are the Fresnel coefficients of each CW array of thickness $(P_z - h)$ far from the resonance (here we assume that r = 0 in a first approximation), and $\alpha = [-\gamma_r(r + t)]^{1/2}$ depends on the radiative decay rate γ_r and quantifies the coupling between propagating waves and the resonance. The quantities with indices are schematically represented in Figure 1b: A_k stands for the amplitude of the nth resonance, $S^{\pm}_{k,l}$ are the incoming and outgoing waves, and all these terms must be understood as being equal to zero if their index is smaller than 1 or exceeds the number of layers. We use the normalization conventions adopted by many authors in the past,[23−25] with $|A_k|^2$ representing the energy stored in the resonator and $|S^{\pm}_{k,l}|^2$ is the power carried by the propagating waves. Last, κ, κ', ..., $\kappa^{(i-1)}$ denote the evanescent coupling between first, second, ..., and ith neighbors, respectively. These constants have the form $U\exp[-d(\varepsilon_{HSQ})^{1/2}/V]$, where d is the distance between neighbors ($d = h$, $P_z + h$, and $2P_z + h$ for κ, κ', and κ''), U = 150 THz, and V = 230 nm. These last two parameters were determined by fitting eq 1 with the full-wave simulations discussed above and were assumed to be independent of the number of layers and of the distance between neighbors (in other words, we use the same values U = 150 THz and V = 230 nm throughout the study). Beside U and V, the only fitting parameters used in the calculations are those describing the Lorentzian response of the single CW layer: $\omega_0 = 2\pi \times 150$ THz, Γ_{tot} = 110 THz, and γ_r = 85 THz.

Figures 2b and 3b show the excellent agreement between the temporal coupled mode theory and the full-wave simulations of Figures 2a and 3a. It may be argued that the theory tends to overestimate the frequencies of the different resonances of Figure 3a, but it correctly predicts the existence of two transmission minima regardless of the number of layers of the structure.

Having validated the model, we can now use this tool to understand the details of the transmission. In Figure 3c, we compare the theoretical transmission of the four-layer structure according to eq 1 with the output of the same equations when the third- and second-neighbor coupling constants κ'' and κ' are successively disabled. Setting κ'' = 0 narrows the separation between the peaks and reduces their amplitude; however, it does not fundamentally modify the aspect of the spectrum (light blue curve). This result can be understood by the fact that κ'' is a small perturbative correction to the total transmission since it is exponentially smaller than κ' and κ. The influence of κ' on the system is much more dramatic since turning off this factor produces a transmission spectrum with three peaks (gray curve) instead of the two predicted by the full theory and the full-wave simulations. In other words, the coupling between second neighbors plays a central role in the response of the four-layer MM: it is the constructive and destructive interferences resulting from these interactions that predominantly contribute to the formation of two well-defined minima in the transmission spectra despite the fact that the actual number of eigenmodes of the system is higher.

Thus, the response of the multilayer MM is intrinsically nonlocal. We have then evaluated the consequences of this complex interplay on the tolerance of the structure to fabrication defects by introducing different types of disorder in eq 1. In Figure 3d, the transmission spectra of an ideal four-layer MM is compared with the response of several imperfect structures: one where each layer has a slightly different resonance frequency ω_0 (red curve), another characterized by a distribution of coupling constants κ' (green curve), and a last one that combines the two types of inhomogeneities (yellow curve). Clearly, it is the first type of disorder (i.e., the introduction of a frequency detuning between the layers) that is the most disruptive since one can observe the appearance of secondary peaks on the low-energy side of the spectrum. Nevertheless, all transmission spectra have two minima that resemble those of the ideal structure, indicating that the MM is very robust to disorder that may arise during the fabrication process. We thus conclude that the nonlocal response of the MM has a powerful stabilizing effect: because the transmission results from multiple contributions, the net effect of

DOI: 10.1021/acsphotonics.5b00180
ACS Photonics 2015, 2, 1129−1134

imperfections is small because their weight is mitigated by all the factors contributing to the overall response of the structure. It should also be noted that the third-neighbor interactions, which seemed to have a negligible influence on the ideal structure (Figure 3c), play an important role in stabilizing the system: by repeating the calculations with disorder without third-neighbor coupling (that is, by setting κ'' to zero), the resulting spectrum is significantly different from the ideal one (gray dashed curve).

The dynamic described here has a broader validity, as it corresponds to the problem of a finite chain of interacting resonators where a certain amount of stochastic disorder is introduced. Similar behaviors have been noticed in other contexts, from various optical cavities[26] to strong-coupling schemes.[27] Moreover, the existence of two transmission minima in multilayer MMs has already been noted by others[16] but never justified to the best of our knowledge.

All the calculations presented in Figure 3 have been performed with a separation distance h = 50 nm between adjacent layers. We now complete this description by presenting the theoretical transmission spectra of four-layer structures with h varying from 10 to 500 nm (Figure 4a). The

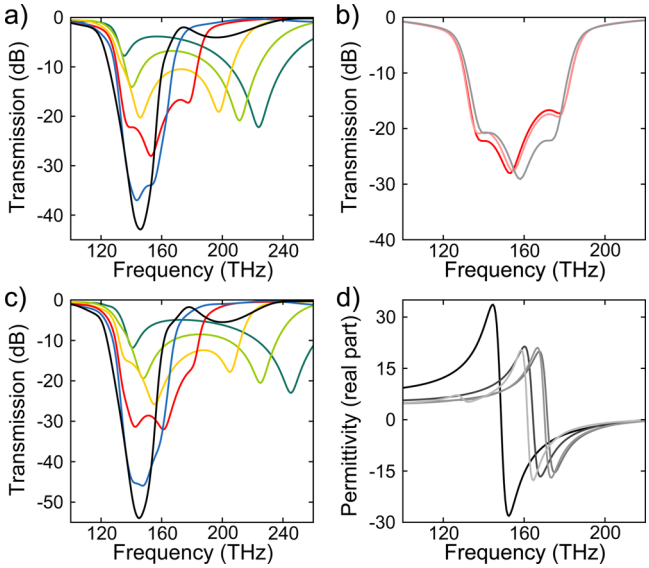

Figure 4. (a) Transmission spectrum of the four-layer structure as the separation distance h is successively set to 10 nm (deep green), 50 nm (light green), 100 nm (yellow), 200 nm (red), 350 nm (blue), and 500 nm (black). The parameters of each layer are the same as those considered in Figures 2 and 3. (b) Transmission for h = 200 nm (red curve, same spectrum as in part a) compared with the calculations with third-neighbor coupling disabled (κ'' = 0, pink curve) and with both third- and second-neighbor interactions disabled (κ'' = κ' = 0, gray curve). (c) Same as part a for a five-layer structure. (d) Real part of the effective permittivity when the number of layers increases from 1 to 5 (from black to light gray). The separation distance between layers is h = 50 nm. All panels show the output of the temporal coupled mode theory. We have verified that these results agree well with full-wave simulations.

curves evolve from the distinct two-peak signature discussed previously to a more complex shape for separation distances h > 100 nm, indicating that the second- and third-neighbor interactions become too weak to fully stabilize the structure. Eventually, as h further increases, the system tends to a stack of uncoupled layers, but the spectra do not simplify into a single peak because new interference effects arise such as Bragg resonance reflections.

The presence of more than two minima in the spectra does not imply that the distant-neighbor interactions can be completely neglected. For example, Figure 4b shows that the transmission spectrum with three peaks obtained for h = 200 nm changes noticeably if one successively disables κ'' and κ' in the calculations, just as we have seen with h = 50 nm in Figure 4c. The separation distance beyond which the influence of κ'' can be totally neglected is h = 350 nm (result not shown here), a value significantly larger than the characteristic length $V/(\varepsilon_{HSQ})^{1/2}$ = 164 nm that defines the exponential decay of the coupling parameters κ, κ', and κ''.

In summary, distant-neighbor interactions have a marked influence on the spectra even for well-separated layers. However, it is only for the most densely packed structures that these interactions fully stabilize the system and produce a transmission spectrum with the recognizable two-peak signature as a result. The separation distance h above which the stabilizing effect wanes depends on the number of layers involved in the transmission. We have verified this trend by repeating the calculations of Figure 4a with an additional fifth layer on the stack. In this case, shown in Figure 4c, the transition between a spectrum with two peaks and a spectrum with three minima occurs for h values between 50 and 100 nm, as opposed to 100−150 nm for the four-layer structure of Figure 4a. This result can be intuitively understood by the fact that, as more layers are added on the system, stronger interactions are needed to maintain two peaks in the spectra since the actual number of eigenmodes increases and the coupling between more and more distant neighbors tends to zero.

As a corollary, even the most strongly interacting structures eventually transition from a two-peak signature to multiple minima as additional planes of CWs are added to the system. This particularity prevents the effective parameters of CW metamaterials from quickly converging toward a bulk value. Figure 4d illustrates this point with a plot of the effective permittivity for a separation distance h = 50 nm, as seen from outside the structures (i.e., the permittivity of an equivalent local medium producing the same transmission and reflection coefficients, a full analysis of the nonlocal parameters being beyond the scope of this study). The permittivity seems to gradually converge, only to diverge again when the fifth layer is added because the stabilizing effects of distant-neighbor coupling become less efficient (Figure 4a and c). This behavior indicates a nonmonotonic convergence that will eventually occur in the asymptotic limit of a large number of periods. It should be noted that a slow convergence of the effective parameters has also been noted for other types of optical MMs with strongly interacting layers, such as fishnet structures.[28]

To verify these predictions, we have fabricated three-dimensional samples by adopting a layer-by-layer strategy. Each array of CWs was obtained by electron-beam lithography, metal deposition, and lift-off and subsequently coated by a film of 100 nm of HSQ. The latter step was achieved by spin-coating liquid HSQ onto the sample and hard-baking it at 400 C for 1 h. We were able to control the alignment of the different levels of CWs with a precision on the order of tens of nanometers by using alignment marks at each step of electron-beam lithography.

We first examine the evolution of the transmission spectrum as a function of the number of layers. To this end, we fabricate

DOI: 10.1021/acsphotonics.5b00180
ACS Photonics 2015, 2, 1129−1134

a four-layer structure with the same geometrical parameters as those used in the simulations of Figure 3a and measure its response upon completion of each level. The transmission spectra were taken with a Variant FTIR spectrometer coupled with an optical microscope equipped with Cassegrain optics. In this setup, the incoming light is focused on the sample with a range of angles between 15 and 30 degrees with respect to the normal direction (again, we remind the reader that the numerical and theoretical data of Figures 2−4 were obtained for normal incidence, but we have verified that they also hold for oblique illumination). As in the simulations, the spectra are taken after applying HSQ on the topmost CW layer so as to homogenize the structure. The finished four-layer sample is shown on the SEM micrograph of Figure 5a, revealing that all

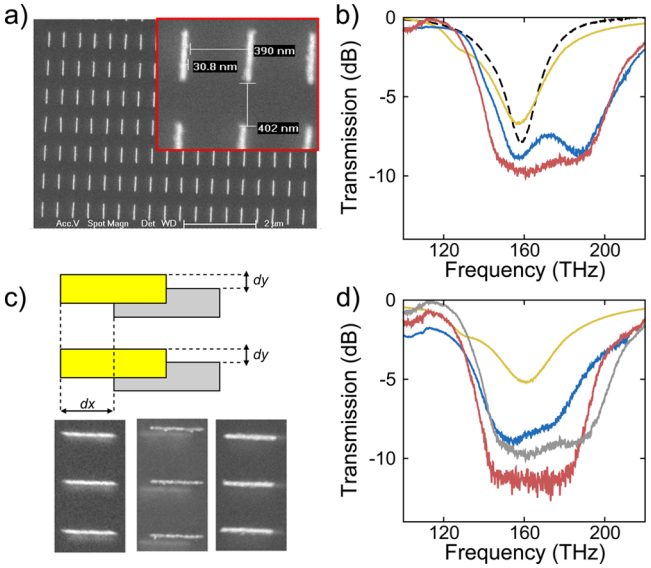

Figure 5. (a) SEM micrograph of a four-layer CW metamaterial (CW dimensions: 440 × 30 × 50 nm; vertical separation distance: h = 50 nm). The close-up view demonstrates that the different planes of CWs are perfectly aligned since the topmost array masks all the underlying layers. (b) Transmission spectrum of the structure after completion of the first, second, third, and fourth CW layer (black dashed, yellow, blue, and red curves, respectively). (c) SEM micrographs of a misaligned structure at various stages of fabrication (from left to right: after fabrication of the second, third, and fourth layer). The schematic on the same panel shows the notation used in the text to describe the misalignments between adjacent planes of CWs. (d) Transmission spectrum of the misaligned structure after completion of the second, third, and fourth CW layers (yellow, blue, and red curves, respectively). As a comparison we also reproduce the response of the aligned four-layer structure of part b (in gray).

levels are perfectly aligned. The results of the experiment are presented in Figure 5b and are in good agreement with the numerical and theoretical predictions of Figure 3. In particular, we see that all spectra are characterized by two transmission minima regardless of the number of layers involved in the transmission even though those minima are not as pronounced as in the calculations. We attribute this difference to the fact that the experimental CWs have a much lower quality factor because of their surface roughness. Note also that there are hints of additional subpeaks on the low-energy side of some spectra, which is in line with the theoretical results of Figure 3d that predicted the existence of such features in the presence of imperfections.

We next repeat the experiment with deliberately misaligned structures. The geometrical parameters are the same as above except that we intentionally introduce longitudinal and lateral shifts dx_n and dy_n between the CWs of the nth and $(n-1)$th layers. In Figure 5c, for example, we consider the case of a structure with misalignments dx_1 = 0, dy_1 = 20 nm; dx_2 = 90, dy_2 = 50 nm; and dx_3 = 100, dy_3 = 0 nm. Several fabrication steps are shown in Figure 5c, while the FTIR transmission spectra recorded after completion of each layer are shown in Figure 5d. For the sake of comparison, the transmission spectrum of the aligned four-layer structure of Figure 5b is also represented: one can see that its response is similar to that of the highly imperfect structure, confirming our earlier predictions that the response of multilayer CW metamaterials is robust to fabrication defects.

To experimentally verify that this tolerance to experimental errors arises from the nonlocal response of the sample, we present in Figure 6 the transmission spectra of bilayer

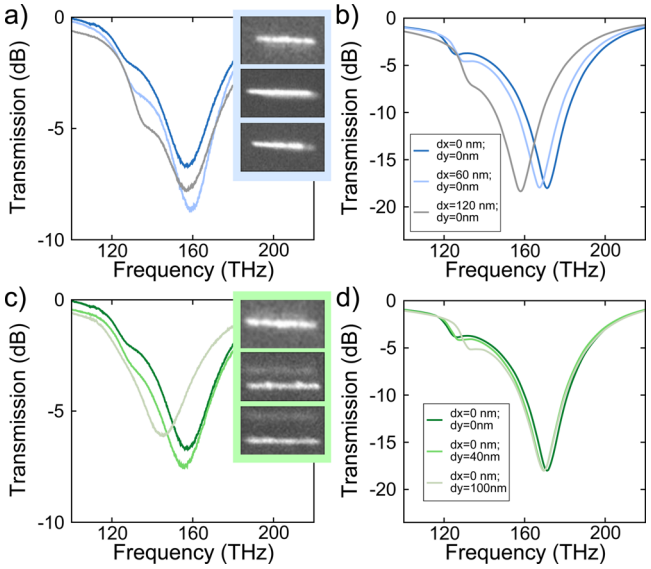

Figure 6. (a) Experimental transmission spectra of three bilayer structures with increasing longitudinal misalignments dx. (b) Corresponding full-wave simulations, with a legend indicating the value of the misalignments. (c) Experimental transmission spectra of three bilayer structures with increasing lateral misalignments dy. (d) Corresponding full-wave simulations, with a legend indicating the value of the misalignments. Insets: SEM close-ups of the structures. The CW dimensions are as always 440 × 30 × 50 nm, while the vertical separation distance is h = 50 nm (or, equivalently, P_z = 100 nm).

structures with either lateral or longitudinal shifts between the two planes of CWs. The properties of these structures are very sensitive to misalignment: for example, the amplitude of the low-frequency peak increases with the longitudinal shift dx (Figure 6a), while the position of both peaks fluctuates when a lateral shift dy is induced (Figure 6c). Moreover, these experimental trends are not fully reproduced by the full-wave simulations of Figure 6b and d, and we attribute this disagreement mainly to the significant surface roughness of the top metalization that tends to shift and damp the resonances of individual CWs. These results clearly show the high sensitivity of bilayer structures to fabrication errors: contrarily to three- and four-layer samples, the bilayer structure has no second- and third-neighbor interactions to stabilize its

DOI: 10.1021/acsphotonics.5b00180
ACS Photonics 2015, 2, 1129−1134

response. It should be noted that the sensitivity of bilayer structures to alignment has been exploited to engineer their resonances at microwave frequencies.[29,30]

In conclusion, we have elucidated the details of the transmission through three-dimensional infrared MMs made of stacks of gold CWs and illustrated the key role played by nonlocal interactions between distant neighbors in these structures. Interestingly, this behavior relaxes the fabrication tolerances because it has a stabilizing effect on the response of the sample that is all the more pronounced because the different planes of the CWs are close to each other. It is probable that most optical MMs characterized by strongly interacting layers are governed by similar effects; in this regard, our findings emphasize the relevance of recent studies dedicated to extract the effective parameters of metamaterials with nonlocal retrieval methods.[31−33]

AUTHOR INFORMATION

Corresponding Author

*E-mail (A. Degiron): aloyse.degiron@u-psud.fr.

Notes

The authors declare no competing financial interest.

ACKNOWLEDGMENTS

This work was supported by the French National Research Agency (ANR Metaphotonique, contract number 7452RA09) and also partly supported by the French RENATECH network. The sample fabrication has been performed at the nanocenter CTU-IEF-Minerve, which was partially funded by the Conseil Général de l'Essonne.

REFERENCES

(1) Soukoulis, C. M.; Wegener, M. Past achievements and future challenges in the development of three-dimensional photonic metamaterials. *Nat. Photonics* **2011**, *5*, 523−530.

(2) Valentine, J.; Zhang, S.; Zentgraf, T.; Ulin-Avila, E.; Genov, D. A.; Bartal, G.; Zhang, X. Three-dimensional optical metamaterial with a negative refractive index. *Nature* **2008**, *455*, 376−379.

(3) Dolling, G.; Enkrich, C.; Wegener, M.; Soukoulis, C. M.; Linden, S. Simultaneous Negative Phase and Group Velocity of Light in a Metamaterial. *Science* **2006**, *312*, 892−894.

(4) Zhou, Y.; Chen, X. Y.; Fu, Y. H.; Vienne, G.; Kuznetsov, A. I.; Luk'yanchuk, B. Fabrication of large-area 3D optical fishnet metamaterial by laser interference lithography. *Appl. Phys. Lett.* **2013**, *103*, 123116.

(5) Chanda, D.; Shigeta, K.; Gupta, S.; Cain, T.; Carlson, A.; Mihi, A.; Baca, A. J.; Bogart, G. R.; Braun, P.; Rogers, J. A. Large-area flexible 3D optical negative index metamaterial formed by nanotransfer printing. *Nat. Nanotechnol.* **2011**, *6*, 402−407.

(6) Gansel, J. K.; Thiel, M.; Rill, M. S.; Decker, M.; Bade, K.; Saile, V.; von Freymann, G.; Linden, S.; Wegener, M. Gold Helix Photonic Metamaterial as Broadband Circular Polarizer. *Science* **2009**, *325*, 1513−1515.

(7) Vignolini, S.; Yufa, N. A.; Cunha, P. S.; Guldin, S.; Rushkin, I.; Stefik, M.; Hur, K.; Wiesner, U.; Baumberg, J. J.; Steiner, U. A 3D Optical Metamaterial Made by Self-Assembly. *Adv. Mater.* **2012**, *24*, OP23−OP27.

(8) Jacob, Z.; Kim, J.-Y.; Naik, G. V.; Boltasseva, A.; Narimanov, E. E.; Shalaev, V. M. Engineering photonic density of states using metamaterials. *Appl. Phys. B: Lasers Opt.* **2010**, *100*, 215−218.

(9) Leonhardt, U.; Philbin, T. G. Transformation Optics and the Geometry of Light. *Prog. Opt.* **2009**, *53*, 69−152.

(10) Ergin, T.; Stenger, N.; Brenner, P.; Pendry, J. B.; Wegener, M. Three-Dimensional Invisibility Cloak at Optical Wavelengths. *Science* **2010**, *328*, 337−339.

(11) Valentine, J.; Li, J.; Zentgraf, T.; Bartal, G.; Zhang, X. An optical cloak made of dielectrics. *Nat. Mater.* **2009**, *8*, 568−571.

(12) Gabrielli, L. H.; Cardenas, J.; Poitras, C. B.; Lipson, M. Silicon nanostructure cloak operating at optical frequencies. *Nat. Photonics* **2009**, *3*, 461−463.

(13) Shalaev, V. M.; Cai, W.; Chettiar, U. K.; Yuan, H.-K.; Sarychev, A. K.; Drachev, V. P.; Kildishev, A. V. Negative index of refraction in optical metamaterials. *Opt. Lett.* **2005**, *30*, 3356−3358.

(14) Dolling, G.; Enkrich, C.; Wegener, M.; Zhou, J. F.; Soukoulis, C. M.; Linden, S. Cut-wire pairs and plate pairs as magnetic atoms for optical metamaterials. *Opt. Lett.* **2005**, *30*, 3198−3200.

(15) Liu, N.; Guo, H.; Fu, L.; Kaiser, S.; Schweizer, H.; Giessen, H. Three-dimensional photonic metamaterials at optical frequencies. *Nat. Mater.* **2008**, *7*, 31−37.

(16) Larouche, S.; Tsai, Y.-J.; Tyler, T.; Jokerst, N. M.; Smith, D. R. Infrared metamaterial phase holograms. *Nat. Mater.* **2012**, *11*, 450−454.

(17) Liu, N.; Guo, H.; Fu, L.; Kaiser, S.; Schweizer, H.; Giessen, H. Plasmon Hybridization in Stacked Cut-Wire Metamaterials. *Adv. Mater.* **2007**, *19*, 3628−3632.

(18) Liu, N.; Fu, L. W.; Kaiser, S.; Schweizer, H.; Giessen, H. Plasmonic Building Blocks for Magnetic Molecules in Three-Dimensional Optical Metamaterials. *Adv. Mater.* **2008**, *20*, 3859−3865.

(19) Decker, M.; Zhao, R.; Soukoulis, C. M.; Linden, S.; Wegener, M. Twisted split-ring-resonator photonic metamaterial with huge optical activity. *Opt. Lett.* **2010**, *35*, 1593−1595.

(20) http://www.ansys.com/Products/Simulation+Technology/Electronics/Signal+Integrity/ANSYS+HFSS.

(21) Kanté, B.; de Lustrac, A.; Lourtioz, J. M.; Gadot, F. Infrared cloaking based on the electric response of split ring resonators. *Opt. Express* **2008**, *16*, 6774−6784.

(22) Haus, H. A. *Waves and Fields in Optoelectronics*; Prentice Hall: Englewood Cliffs, NJ, 1984; pp 197−207.

(23) Suh, W.; Solgaard, O.; Fan, S. Displacement sensing using evanescent tunneling between guided resonances in photonic crystal slabs. *J. Appl. Phys.* **2005**, *98*, 033102.

(24) Fan, S.; Suh, W.; Joannopoulos, J. D. Temporal coupled-mode theory for the Fano resonance in optical resonators. *J. Opt. Soc. Am. A* **2003**, *20*, 569−572.

(25) Lepetit, T.; Akmansoy, E.; Ganne, J.-P.; Lourtioz, J.-M. Resonance continuum coupling in high-permittivity dielectric metamaterials. *Phys. Rev. B: Condens. Matter Mater. Phys.* **2010**, *82*, 195307.

(26) Benisty, H. J. Dark modes, slow modes, and coupling in multimode systems. *J. Opt. Soc. Am. B* **2009**, *26*, 718−724.

(27) Houdré, R.; Stanley, R. P.; Ilegems, M. Vacuum-field Rabi splitting in the presence of inhomogeneous broadening: Resolution of a homogeneous linewidth in an inhomogeneously broadened system. *Phys. Rev. A: At., Mol., Opt. Phys.* **1996**, *53*, 2711−2715.

(28) Zhou, J.; Koschny, T.; Kafesaki, M.; Soukoulis, C. M. Negative refractive index response of weakly and strongly coupled optical metamaterials. *Phys. Rev. B: Condens. Matter Mater. Phys.* **2009**, *80*, 035109.

(29) Zhou, J.; Economou, E.; Koschny, T.; Soukoulis, C. M. Unifying approach to left-handed material design. *Opt. Lett.* **2006**, *31*, 3620−3622.

(30) Burokur, S. N.; Sellier, A.; Kanté, B.; de Lustrac, A. Symmetry breaking in metallic cut wire pairs metamaterials for negative refractive index. *Appl. Phys. Lett.* **2009**, *94*, 201111.

(31) Andryieuski, A.; Ha, S.; Sukhorukov, A. A.; Kivshar, Y. S.; Lavrinenko, A. V. Bloch-mode analysis for retrieving effective parameters of metamaterials. *Phys. Rev. B: Condens. Matter Mater. Phys.* **2012**, *86*, 035127.

(32) Liu, X.-X.; Alù, A. Generalized retrieval method for metamaterial constitutive parameters based on a physically driven homogenization approach. *Phys. Rev. B: Condens. Matter Mater. Phys.* **2013**, *87*, 235136.

(33) Grigoriev, V.; Demésy, G.; Wenger, J.; Bonod, N. Singular analysis to homogenize planar metamaterials as nonlocal effective media. *Phys. Rev. B: Condens. Matter Mater. Phys.* **2014**, *89*, 245102.

DOI: 10.1021/acsphotonics.5b00180
ACS Photonics 2015, 2, 1129−1134